Thermotropic Phase Behavior and Stability of Monosialoganglioside Micelles in Aqueous Solution

Mitsuhiro Hirai, Toshiharu Takizawa, Sadato Yabuki, Yoshiro Nakata, and Kouhei Hayashi
Department of Physics, Gunma University, Maebashi 371, Japan.

ABSTRACT The thermotropic phase behavior of monosialoganglioside in a dilute aqueous dispersion at pH 6.8 was measured by using synchrotron radiation small-angle x-ray scattering and was analyzed by a shell-modeling method. Previous calorimetric studies on ganglioside systems have shown quite different thermotropic behaviors from other biological lipid systems, however, the details have still been ambiguous. Because of high statistical data and a shell-modeling analysis, we could elucidate the internal structural change of monosialoganglioside micelle induced by the elevation of temperature from 6 to 60°C, that is, the shrinkage of the hydrophilic region and the slight expansion of the hydrophobic region occurring simultaneously, accompanying the elongation of the axial ratios of the ellipsoidal micelles. The model structures obtained explain the changes in the experimental scattering curves, the distance distribution functions, and the gyration radii. In addition we have also found an evident thermal hysteresis in the scattering curves and in the structural parameters. The present result suggests that the thickness of the hydrophilic region, namely, the conformation of oligosaccharide chains, is sensitive to a change of temperature.

INTRODUCTION

Physiological functions of gangliosides have been attracting scientific concerns and have been studied intensively (Hakomori, 1986; Svennerholm et al., 1994). The gangliosides, the most complex of the sphingolipids, contain ceramide linked to an oligosaccharide chain containing one or more *N*-acetylneuraminic acid (sialic acid) residues. Although they are found in much smaller quantities in most cell types, the gangliosides are most abundant in the nerve cell membrane (Makita and Taniguchi, 1985). Through molecular recognition by the various oligosaccharide chains, they are concerned in various functions, ie, the cell differentiation and the biotransduction of membrane-mediated information (Hakomori, 1981), the cell growth and the self organization of tissues (Spiegel and Fishman, 1987), and the immune response (Marcus, 1984).

According to the increase of the evidence of the important functions of gangliosides, many studies have been carried out to clarify physicochemical properties (especially aggregative properties) of gangliosides by using light, neutron, and x-ray scattering techniques (Cantù et al., 1986; Corti and Cantù, 1990) and by using analytical chromatography (Robert and Robert, 1964; Formisano et al., 1979; Ulrich-Bott and Wiegandt, 1984). Although gangliosides form micellar structures in many cases in these studies, the intramicellar structures still seem to be ambiguous. Because of high statistical data from synchrotron radiation x-ray scattering we will discuss the widths of the hydrophilic head and hydrophobic tail regions of the ganglioside micelles, and the thermotropic change of those regions in detail. The present findings show a characteristic hydrodynamic property of gangliosides differing from other amphipathic lipids, which would relate to physiological functions of gangliosides.

Received for publication 25 September 1995 and in final form 4 January 1996.

Address reprint requests to Dr. Mitsuhiro Hirai, Associate Professor, Department of Physics, Gunma University, 4–2 Aramaki, Maebashi 371, Japan. Tel.: +81 272-20-7554; Fax: +81 272-20-7405; E-mail: hirai@la.gunma-u.ac.jp.

0006-3495/96/04/1761/08 $2.00

MATERIALS AND METHODS

Ganglioside samples

The sample used was monosialoganglioside (G_{M1}) from bovine brain, which was purchased from SIGMA Chemical Ltd. USA and used without further purification. The G_{M1} powder with 0.5% w/v was dissolved in 1/15 M phosphate buffer (Na_2HPO_4/KH_2PO_4), adjusted to pH 6.8, and used for the scattering experiments.

Small-angle x-ray scattering measurements

Small-angle x-ray scattering experiments were performed by using the synchrotron radiation small-angle x-ray scattering spectrometer installed at the BL10C line of the 2.5 GeV storage ring at the Photon Factory at the National Laboratory for High Energy Physics, Tsukuba, Japan. The details of the instruments are described elsewhere (Ueki et al., 1985). The x-ray wavelength, the sample-to-detector distance, and the exposure time were 1.49 Å, 87 cm, and 100 s, respectively. The integrated exposure time was 1200 s. The temperature of the sample was varied in the range of 6 to 60°C by a thermostat within precision below 0.5°C.

Scattering data and modeling analyses

The scattering data were analyzed based on the standard methods (Hirai et al., 1993), and the shell-modeling analysis using the formulations defined previously (Hirai et al., 1994, 1995) was carried out to fit the experimental data, as shown below. The beginning of the scattering curve $I(q)$ is known to depend on the Guinier equation in the form

$$I(q) = I(0)\exp(-q^2R_g^2/3) \quad (1)$$

where $I(0)$ designates the zero-angle scattering intensity, R_g the radius of gyration, and the magnitude of scattering vector is defined by $q = (4\pi/\lambda)\sin(\theta/2)$($\theta$, the scattering angle; λ, the wavelength). By using the Guinier plot ($\ln(I(q))$ vs. q^2) we can determine the values of both $I(0)$ and R_g, where we used the data sets in the q interval of 0.020–0.025 Å^{-1} for this plot. The distance distribution function $p(r)$ was obtained by the Fourier inversion of the scattering intensity $I(q)$ as

$$p(r) = \frac{2}{\pi}\int_0^\infty rqI(q)\sin(rq)\,dq \qquad (2)$$

The $p(r)$ function reflects the particle shape, the intraparticle scattering density distribution, and the interparticle translational correlation (Glatter, 1982). For the calculation of the $p(r)$ function, the extrapolation of the small-angle data sets by using the Guinier plot and the modification of the scattering intensity as

$$I'(q) = I(q)\exp(-kq^2) \qquad (3)$$

(k is the artificial damping factor) were employed to reduce the Fourier truncation effect. The maximum dimension D_{max} of the particle was estimated from the $p(r)$ function satisfying the condition $p(r) = 0$ for $r > D_{max}$.

The following indirect Fourier transform method, the so-called Glatter's method, (Glatter, 1982) was also applied to eliminate some inherent artifacts on the estimation of R_g and I_{total} when using the Guinier approximation. R_g and I_{total} are given as

$$I_{total} = \int_0^{D_{max}} p(r)\,dr \qquad (4)$$

and

$$R_g^2 = \int_0^{D_{max}} p(r)r^2\,dr \Big/ 2\int_0^{D_{max}} p(r)\,dr \qquad (5)$$

Equation 4 was used for normalization of the $p(r)$ functions.

The shell-modeling analysis was also carried out for fitting the experimental data to determine structural parameters. As we have shown elsewhere (Hirai et al., 1994, 1995), based on the convolution theory the spherically averaged scattering function $I(q)$ from of a particle composed of shells with different average scattering densities is simply given as

$$I(q) \propto \langle A(q)A^*(q)\rangle \qquad (6)$$

$$= \int_0^1 \left[3\left\{\frac{\bar{\rho}_1 V_1 j_1(qR_1)}{(qR_1)} + \frac{\sum_{i=2}^{n}(\bar{\rho}_i - \bar{\rho}_{i-1})V_i j_1(qR_i)}{(qR_i)}\right\}\right]^2 dx$$

where $\langle\ \rangle$ means the spherical average of the scattering intensity $I(\mathbf{q})$defined by $A(\mathbf{q})A^*(\mathbf{q})$(the structural factor $A(\mathbf{q})$), $\bar{\rho}_i$ is the average excess scattering density (so-called contrast) of the i th shell with a shape with an ellipsoid of rotation, and j_1 is the spherical Bessel function of the first rank. R_i is defined as

$$R_i = r_i(1 + x^2(\nu_i^2 - 1))^{1/2} \qquad (7)$$

where r_i and ν_i are the semiaxis and the axial ratio for the ith ellipsoidal shell, respectively. Here we assumed the simplified model of a double-shell ellipsoidal structure to fit the experimental scattering data by using Eq. 6. $\bar{\rho}$, r_i, and ν_i are used as fitting parameters. Although this modeling method cannot avoid some systematic disagreement with experimental data at a high angle region because of the simplified model representation as a set of ellipsoids, Eq. 6 is very useful to sort out various models of globular solute particle with a center-symmetrical internal scattering density heterogeneity.

RESULTS

Change of scattering curve and gyration radius

Fig. 1 *A* and Fig.1 *B*, show the temperature dependence of the scattering curve $I(q)$ of the G_{M1} ganglioside aggregates at the first temperature scan and at the second one, respectively. After cooling down the aggregates to 6°C and leaving them for ~2 h, the second scan was started. As there was no difference between the scattering curves just after cooling and at the initial point of the second scan, 2 h was short enough to detect a thermal hysteresis under the present conditions. All scattering curves have evident minimums at q ~0.06 Å^{-1} and bell-shaped peaks at q ~0.1 Å^{-1}, indicating the monodispersion of the ganglioside aggregates to

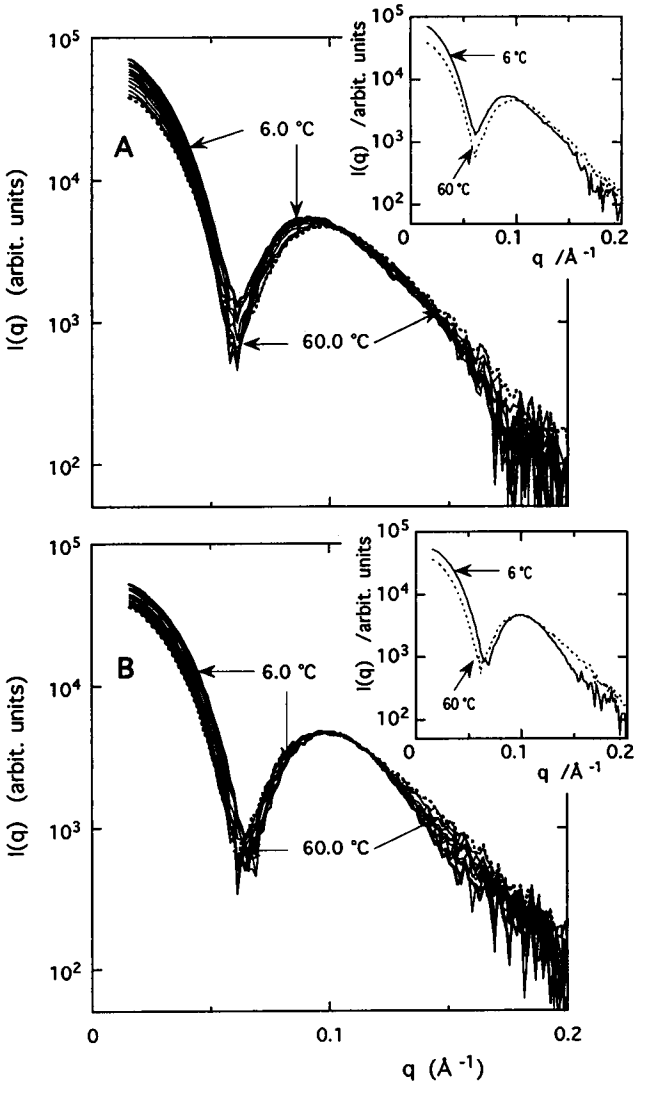

FIGURE 1 Variation of the scattering curve of G_{M1} aggregates in phosphate buffer at pH 6.8. The variation depends on temperatures from 6 to 60°C. *A*, at the first temperature scan; *B*, at the second temperature scan. Thick and dotted lines correspond to the scattering curves of 6°C and 60°C, respectively. Insets in *A* and *B* extract two curves of both these temperatures. Ganglioside concentration is 0.5% w/v.

form globular structures, micelles, in the temperature range of 6 to 60°C. The micelle takes a prolate ellipsoidal shape, as shown in the following modeling analysis. At the first scan the elevation of temperature causes the shift of the position of the bell-shaped peak from 0.092 $Å^{-1}$ to 0.10 $Å^{-1}$, accompanying the change of the ratio of the minimum to the peak in intensity from 0.258 to 0.129. Comparing Fig. 1 *B* with Fig. 1 *A*, we can see the distinct thermal hysteresis of the changing manner of the scattering curve when restarting from 6°C; and the scattering curve of 60°C at the second scan appropriately coincides with that at the first scan.

Fig. 2 shows the temperature dependence of the gyration radius R_g obtained by the Glatter's method using Eq. 5. As is well known, R_g determination using the Guinier equation (Eq. 1) is very conventional and is usually carried out by using the q interval satisfying $qR_g < 1$, which depends on the the shape, the dimension, and the internal scattering density distribution of the objects. However, the use of Eq. 1 is also known to include an inherent systematic error by a Gaussian approximation of small-angle scattering curves. Moreover, in many cases the accuracy of R_g is affected by other factors such as the reasonability of the q interval, the scattering data statistic, and the presence of an interparticle interaction. Actually, because of the presence of sialic acids in ganglioside molecules we observed an evident intermicellar repulsive interaction at the concentration range of 5 to 1.5 w/v %, which seriously deformed the scattering curve at a small-angle region (Hirai et al., 1995). Therefore we selected the concentration of 0.5 w/v % to obtain enough statistics for modeling analyses to avoid an apparent deformation of the scattering curve by the repulsive interaction. As the present q interval of 0.020 to 0.025 $Å^{-1}$ is appropriate, the gyration radius obtained by using Eq. 1 shows the same changing tendency. In comparison with the use of Eq. 1, the Glatter's method is less sensitive to the above ambiguity factors and gives more accurate R_g values because of the use of the total observed scattering curve. At the first scan in Fig. 2 the gyration radius R_g increases once from 51.50.1 Å to 52.60.1 Å in the temperature range of 6 to 35°C and then decreases to 50.90.1 Å. At the second scan the R_g monotonously increases from 47.10.1 Å to 50.00.1 Å. Thus Fig. 2 suggests that the elevation of temperature induces the structural change of the G_{M1} micelle, namely, the change in both the micellar dimension and the intramicellar scattering density distribution, which is also suggested and reasonably explained by the following distance distribution function and modeling analyses. In Fig. 2 the gyration radii estimated from the following double-shell modeling analysis are also shown, where the R_g values and the manner of the changes are in agreement with the above experimental ones.

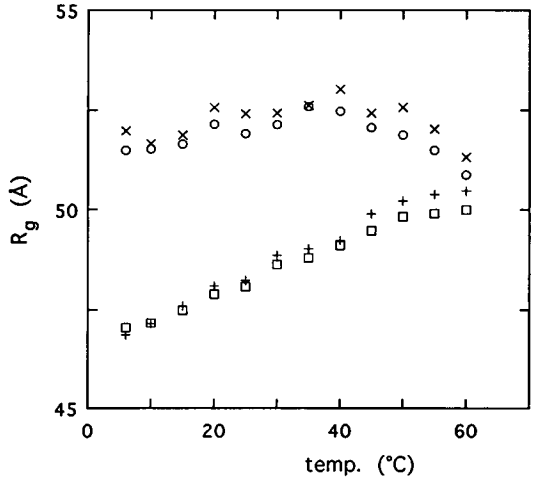

FIGURE 2 Temperature dependence of the gyration radius of the G_{M1} micelle determined by using the Glatter method in Figs. 1 and 3. ○, for the first temperature scan; □, for the second temperature scan. × and + correspond to the gyration radii for the first and second scans obtained from the modeling analysis in Figs. 4 and 5.

Distance distribution function analysis

Fig. 3, *A* and *B*, shows the distance distribution functions $p(r)$ obtained by the Fourier inversion of the scattering curves in Fig. 1, *A* and *B*, respectively. The $p(r)$ profile at low temperatures is characterized by the shoulder of ~28 to 38 Å and the main peak of ~75 Å. In the first scan in Fig. 2 *A*, by the elevation of temperature from 6 to 60°C, the shape of the shoulder becomes a small peak when shifting its peak position from 23.5 Å to 22.2 Å; and the main peak position of 75.8 Å moves once to 77.2 Å and finally to 74.1 Å. At the second scan in Fig. 2 *B*, the shoulder becomes a small peak when shifting its position from 24.7 Å to 22.2 Å, and the main peak position of 72.2 Å moves monotonously to 74.1 Å. Such changes of the $p(r)$ profiles suggest that the temperature elevation induces a rearrangement of the ganglioside molecules in the micelle to enhance the scattering density fluctuation within the micelle. The maximum dimension D_{max} of the G_{M1} micelle at the first scan increases once from 129 Å to 148 Å and decreases to 138 Å. At the second scan the D_{max} monotonously increases from 114 Å to 122 Å. Thus, at the first scan the maximum dimension initially expands, followed by a contraction, and at the second scan a simple expansion occurs, which agrees well with the changing tendencies of the R_g values in both scans in Fig. 2.

Shell-modeling analysis

To discuss such changes in detail we applied the shell-modeling analysis to fit the experimental scattering curves $I(q)$ and the distance distribution functions $p(r)$. Figs. 4 and 5 show the scattering curves $I(q)$ and the $p(r)$ functions for the best fitted models, where the thick and dotted lines correspond to 6°C and 60°C, respectively. The shell-modeling analysis is applicable to the scattering data from the solute particles having an evident heterogeneity of the scat-

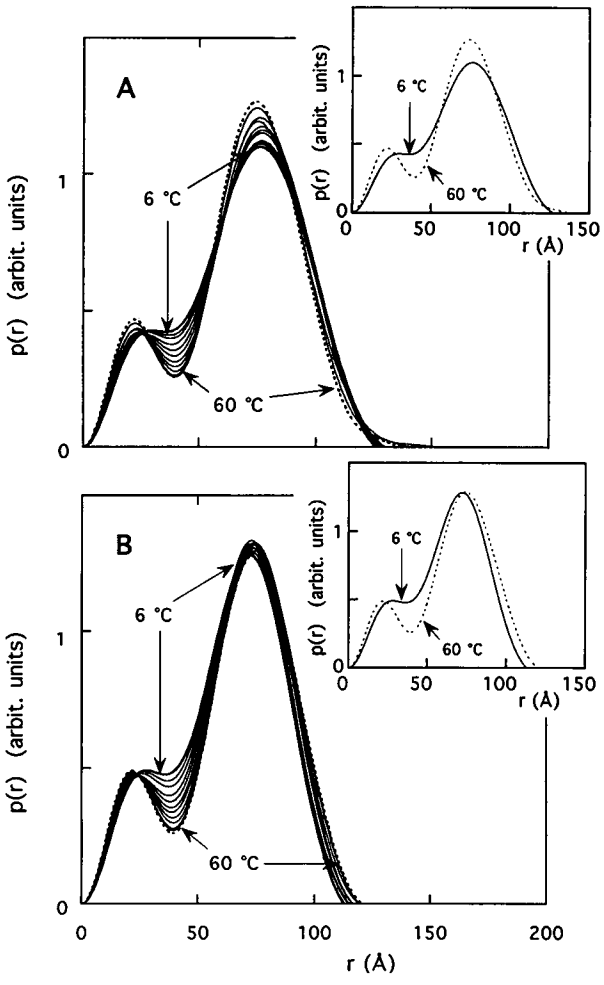

FIGURE 3 Temperature-dependent variation of the distance distribution functions $p(r)$ obtained from the Fourier inversion of the scattering curves in Fig. 1. *A* and *B* as in Fig. 1.

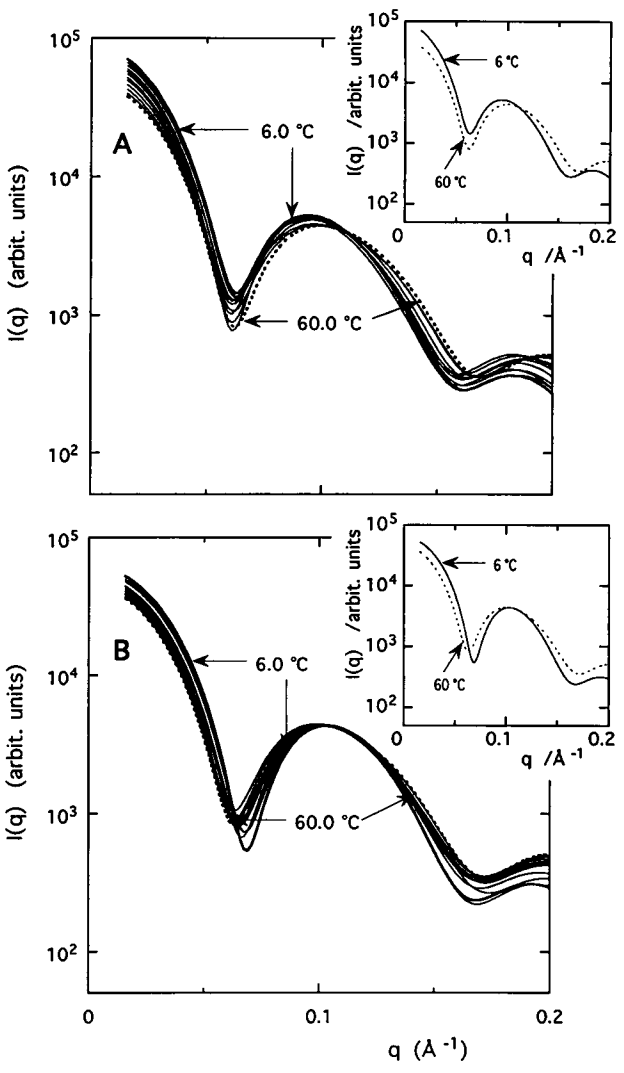

FIGURE 4 Scattering curves obtained from the double-shelled-ellipsoid-model fittings. Thick and dotted lines correspond to the scattering curves of 6°C and 60°C, respectively. Insets in *A* and *B* extract two curves of both these temperatures. *A* and *B* as in Fig. 1.

tering density distribution with a center symmetry (Hirai et al., 1994, 1995). As the G_{M1} ganglioside molecule is composed of a hydrophobic moiety of a ceramide and of a hydrophilic moiety of a oligosaccharide chain with a sialic acid, it is suitable to describe the ganglioside micelle as a double-shelled ellipsoid of rotation that consists of a core surrounded by a shell with different scattering densities. Least-squares fitting parameters used were the core and shell radii, the semiaxial ratios, and the average excess scattering densities compared to the average scattering density of the solvent (so-called contrasts). The reliability factors R, defined by $R = \sum |I_{obs}(q) - I_{model}(q)|/\sum I_{obs}(q)$, are in the range of 0.025 to 0.031 for the presented models. Although there is some disagreement in the $I(q)$ curve over 0.15 $Å^{-1}$ because of the simplicity of the model structure, the $I(q)$ and $p(r)$ profiles in Figs. 4 and 5 well describe the experimental ones shown in Figs. 1 and 3. For example, in Fig. 4 *A*, the optimized model of 6°C has the core and shell radii of 26.7 Å and 47.5 Å, respectively, the semiaxial ratios of 1.63 and 1.53, and the average scattering densities of 0.573 and 1.56, where the scattering densities are relative values to that of the solvent. The optimized model of 60°C is a double-shelled ellipsoid with the core and shell radii of 26.6 Å and 42.9 Å, respectively, the semiaxial ratios of 1.87 and 1.61, and the average scattering densities of 0.592 and 1.55. This indicates that the temperature elevation induces the decrease of the ~4.5-Å width of the oligosaccharide chain length in the hydrophilic region. The R_g values for the above two models are 51.9 Å and 51.3 Å, respectively. These values agree with the experimental values of 51.5 Å and 50.9 Å. The temperature dependence of the R_g for the optimized model in Fig. 2 can also explain that obtained by the experiments.

By using the empirical expressions of a hydrocarbon chain volume and of a critical chain length (Israelachvili et al., 1976) and by considering the apparent atomic volumes of the basic chemical elements (Zamyatin, 1972), we can tentatively estimate the average scattering densities of

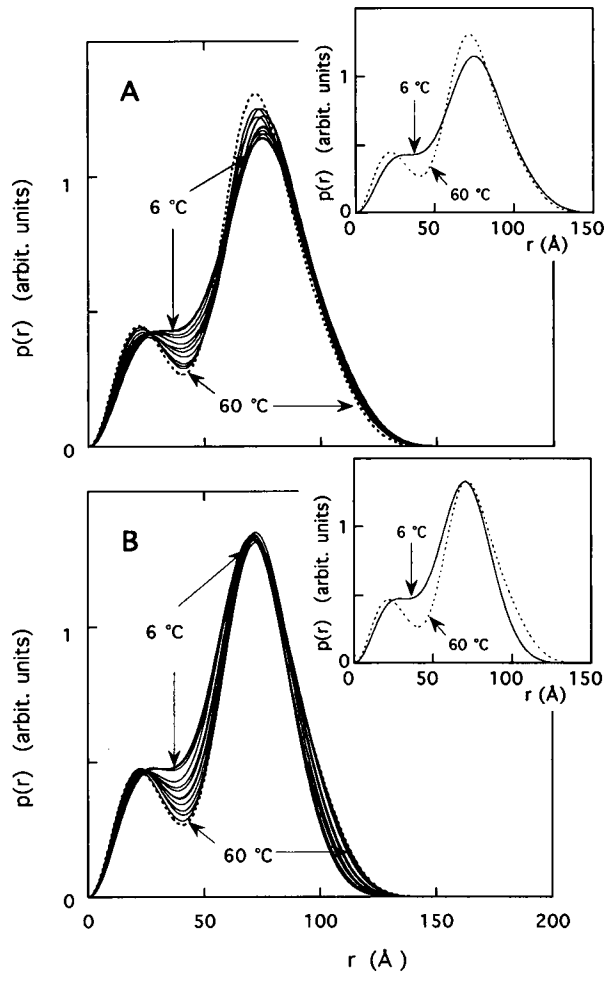

FIGURE 5 Distance distribution functions $p(r)$ obtained from the Fourier inversion of the scattering curves for the best-fitted model structures in Fig. 4. Thick and dotted lines correspond to the $p(r)$ functions of 6°C and 60°C, respectively. Insets in *A* and *B* extract two functions of both of these temperatures. *A* and *B* as in Fig. 1.

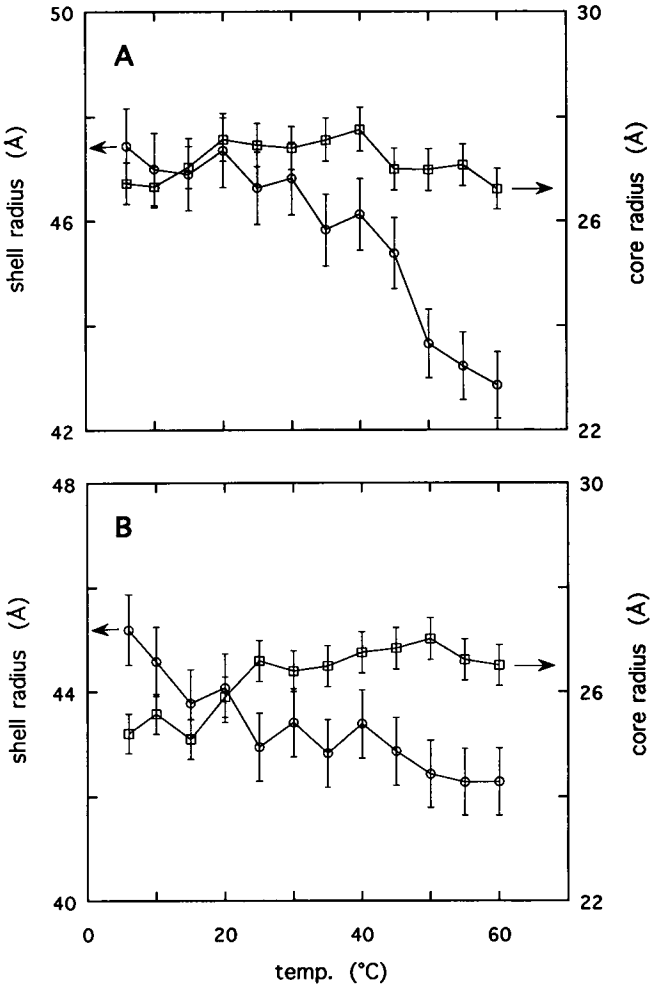

FIGURE 6 Shell and core radii of the ganglioside micelle estimated by the shell-modeling analysis in Fig. 4, plotted against temperature. ○ and □ are the shell and core radii; *A* and *B* as in Fig. 1.

the hydrophilic head and hydrophobic tail of the G_{M1} molecule to be 12.3×10^{10} cm^{-2} and 8.7×10^{10} cm^{-2} (8×10^{10} cm^{-2} for only saturated-hydrocarbon chains C_{18}/C_{20} = 1/1), respectively. The critical chain length of C_{20} is 26.8 Å and the average scattering density of water solvent is 9.4×10^{10} cm^{-2}. When considering the intrinsic experimental limitation from the resolution in the small-angle scattering method and the simplicity of the shell-modeling analysis, the structural parameters obtained on the models are in agreement with the empirical values within the orders.

Temperature dependence of the structural parameters of G_{M1} micelle

The temperature dependence of the structural parameters obtained by the present modeling analysis, the core and shell radii, the semiaxial ratios, and the average excess scattering densities, are summarized in Figs. 6, 7, and 8, respectively. In the first scan in Fig. 6 *A*, the shell radius decreases gradually in the temperature range of 6 to ~40°C and more rapidly above 40°C. The core radius increases slightly in the same range and afterward decreases slightly. Simultaneously, in Fig. 7 *A* the axial ratios of the core and the shell are mostly constant in the temperature range of 6 to 25–30°C and afterward begin to increase. In comparison with the above case, we can recognize some differences between the second scans in Figs. 6 *B* and 7 *B*. Although the core radius shows a similar change, a fast decrease of the shell radius occurs in the temperature range of 6 to ~25°C and a more evident increase of the core radius occurs in the temperature range of 20 to 50°C. The changes of the axial ratios start at 6°C and their increments are greater than those at the first scan. In Fig. 8 the shell scattering densities in both scans are within errors, except for a slight fluctuation at the second scan. At both scans the core densities are also in the range of 6 to ~50°C and take slightly higher values above ~55°C.

The above changes of the structural parameters that depend on temperature suggest that the elevation of tempera-

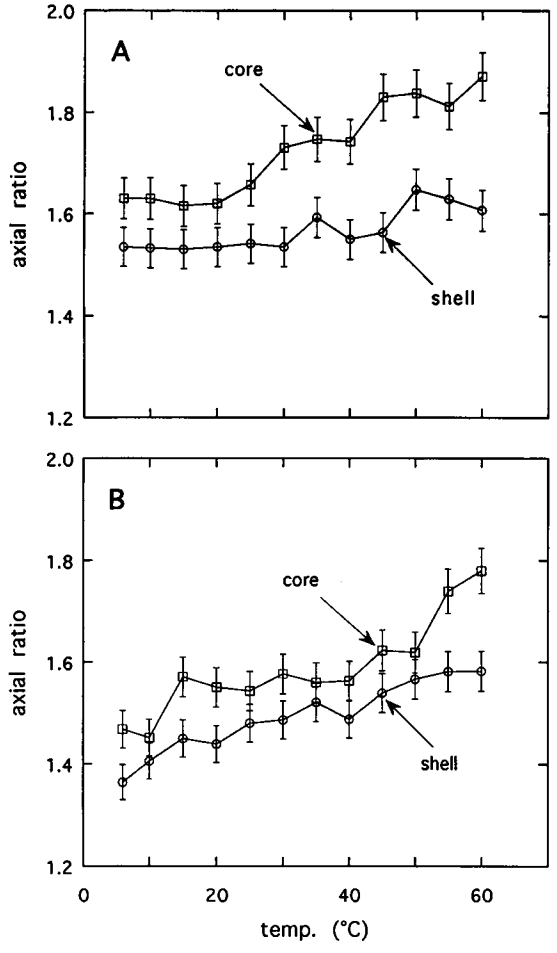

FIGURE 7 Shell and core semiaxial ratios of the ganglioside micelle estimated by the shell-modeling analysis in Fig. 4, plotted against temperature. ○ and □ are the shell and core semiaxial ratios; *A* and *B* as in Fig. 1.

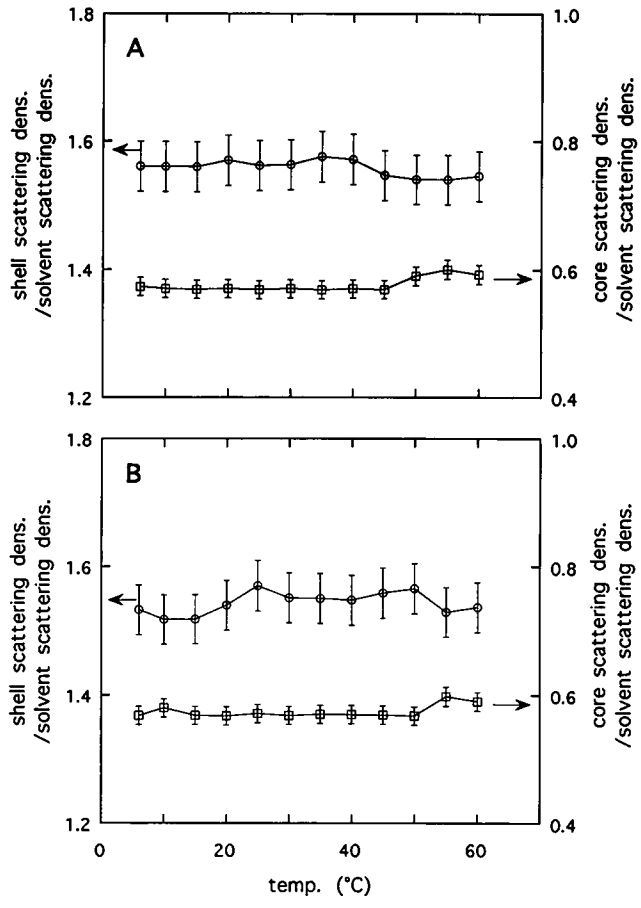

FIGURE 8 Relative values of the scattering densities of the shell and the core of the ganglioside micelle compared with that of the solvent estimated by the shell-modeling analysis in Fig. 4, plotted against temperature. ○ and □ are the shell and core scattering densities; *A* and *B* as in Figure 1.

ture induces the shrinkage of the hydrophilic region and the slight expansion of the hydrophobic region accompanying the elongation of the semiaxial ratios of both regions in the ellipsoidal micelles. The competition between the shrinkage and the expansion result in the complicated characteristics of the thermotropic phase behavior as the observed structural changes in the scattering curve, the R_g value and the $p(r)$ profile.

DISCUSSION

By using high-intensity x ray from a synchrotron radiation source and by using an appropriate shell-modeling analysis, we have shown the thermotropic phase behavior of G_{M1} ganglioside micelles and the changes of the hydrophilic and hydrophobic regions in the micelle, respectively. The structural changes occur on both the micellar shape and the intramicellar structure, especially on the oligosaccharide chain region. The present results are schematically shown in Fig. 9. Gammack (1963) observed that mixed brain gangliosides in dilute aqueous solution form prolate ellipsoidal micelles (axial ratio ~2) by using hydrodynamic measurements. The temperature dependence of the hydrodynamic radius reported in the light scattering study of G_{M1} micellar aqueous solutions (Cantù, 1986) might correspond to that observed at the first scan in the present experiments. Calorimetric studies treating micellar and vesicle dispersions clarified that gangliosides show rather broad endothermal transitions that are very different from those of the membrane phospholipids and that a minor presence of gangliosides in phospholipids greatly affects thermotropic phase transitions (Sillerud et al., 1979; Bach et al., 1982; Maggio et al., 1985; Kojima et al., 1988). Such characteristic thermotropic behaviors would be reflected in the present results showing gradual changes in the scattering curve, the $p(r)$ function, and the R_g value, which can be explained as the changes of the micellar shape and the intramicellar structure, as shown above.

Curatolo et al. (1977) studied broad thermotropic transitions, having two small endothermal peak maxima at 30 and 46°C, of mixed brain gangliosides in a hexagonal phase over the hydration range of 18 to 50 wt %. They showed that even below 30°C the hydrocarbon chains are disordered;

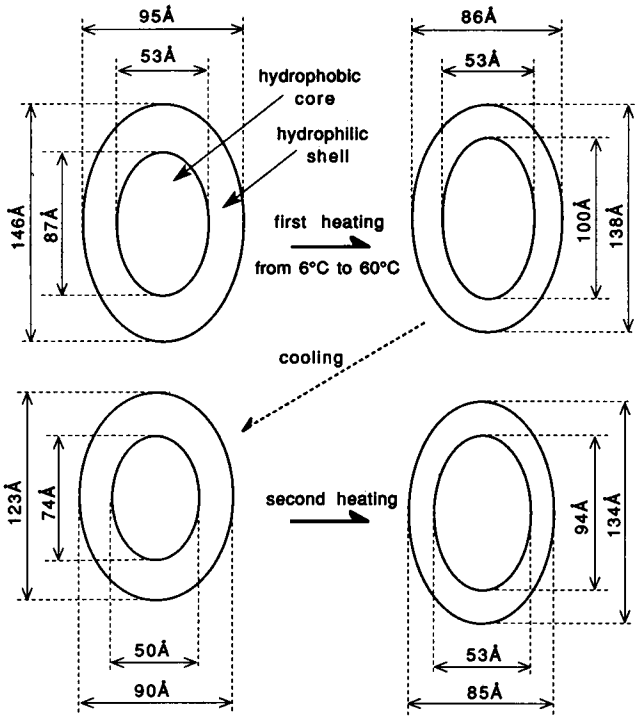

FIGURE 9 Schematic picture of thermal structural transition of G_{M1} micelles. Only the structures at initial and final temperatures in the first and second heating processes are displayed.

and they concluded that the broad thermotropic transitions are not identical to the order-disorder (chain-melting) transitions in phospholipid systems and that these transitions are related to a change from one disordered state to a more disordered state. Moreover, some thermodynamical and experimental considerations suggest that the hydrocarbon chains in micelles essentially contain many gauche-bond configurations (Gruen, 1981; Gruen and Lacey, 1984; Dill et al., 1984). Therefore, the presence of disordered hydrocarbon chains is more probable for the gangliosides in micellar phase, and chain-melting models do not seem to be enough to describe thermotropic transitions of ganglioside micelles. We can assume, therefore, that the present transition behavior of the hydrophobic cores results from some rearrangement of the hydrocarbon chains. This is also suggested by Masserin and Freire (1986) and Masserin et al. (1989).

Recently, for gangliosides (G_{D1a} and mixture)-water systems we have observed two broad endothermal transitions (at ~30 and 50°C) accompanying an evident thermal hysteresis in the thermogram where the hysteresis at 30°C is more evident (Takizawa et al. submitted for publication). The present thermal hysteresis in the scattering curves and in the structural parameters also reflects such tendencies in spite of the use of other ganglioside systems. Further, we assume the changes of the hydrophilic and hydrophobic regions can accompany the extrusion of some amount of intramicellar hydrated water from the hydrophilic region and from the hydrophobic core interface due to the contraction of the oligosaccharide chains. In other words, interactions between boundary water and highly hydrophilic heads of gangliosides can probably appear as some conformational changes of oligosaccharide chains, which might make the thermotropic phase behavior more complex as some variety of the hydrocarbon chain composition (Masserin and Freire, 1986). The high sensitivity in hydrophilic moieties of gangliosides might relate to their various physiological surface events in biomembranes.

We thank Drs. Y. Amemiya and K. Kobayashi of the Photon Factory at the National Laboratory for High Energy Physics for their help with the small-angle scattering instrumentation. This work was performed with the approval of the Photon Factory Programme Advisory Committee (Proposal No. 92–069 and 93G047).

REFERENCES

Bach, D., I. R. Miller, and B.-A. Sela. 1982. Calorimetric studies on various gangliosides and ganglioside-lipid interactions. *Biochim. Biophys. Acta.* 686:233–239.

Cantù, L., M. Corti, S. Sonnino, and G. Tettamanti. 1986. Light scattering measurements on gangliosides: dependence of micellar properties on molecular structure and temperature. *Chem. Phys. Lipids.* 41:315–328.

Corti, M., and L. Cantù. 1990. Application of scattering techniques in the domain of amphiphiles. *Adv. Colloid Interface Sci.* 32:151–166.

Curatolo, W., D. M. Small, and G. G. Shipley. 1977. Phase behavior and structural characteristics of hydrated bovine brain gangliosides. *Biochim. Biophys. Acta.* 468:11–20.

Dill, K. A., D. E. Koppel, R. S. Cantor, J. D. Dill, D. Bendedouch, and S.-H. Chen. 1984. Molecular conformations in surfactant micelles. *Nature.* 309:42–45.

Formisano, S., M. L. Johnson, G. Lee, S. M. Aloj, and H. Edelhoh. 1979. Critical micelle concentrations of gangliosides. *Biochemistry.* 18: 1119–1124.

Gammack, D. B. 1963. Physicochemical properties of ox-brain gangliosides. *Biochim. J.* 88:373–383.

Glatter, O. 1982. Data treatment. *In* Small Angle X-ray Scattering. O. Glatter and O. Kratky, editors. Academic Press, London. 119–196.

Gruen, D. W. R. 1981. The packing of amphiphile chain in a small-spherical micelle. *J. Colloid Interface Sci.* 84:281–283

Gruen, D. W. R., and E. H. B de Lacey. 1984. The packing of amphiphile chains in micelles and bilayers. *In* Surfactants in Solution, Vol. 1. K. L. Mittel, and B. Lindman, editors. Plenum Press, New York. 279–306.

Hakomori, S. 1981. Glycosphingolipids in cellular interaction, differentiation and oncogenesis. *Ann. Rev. Biochem.* 50:733–764

Hakomori, S. 1986. Glycosphingolipids. *Sci. Am.* 254:32–41.

Hakomori, S., and Y. Igarashi. 1993. Gangliosides and glycosphingolipids as modulators of cell growth, adhesion, and transmembrane signaling. *Adv. Lipid Res.* 25:147–162.

Hannun, Y. A., and R. M. Bell. 1989. Functions of sphingolipids and sphingolipid breakdown products in cellular regulation. *Science.* 243: 500–507.

Hansson, H. A., J. Holmgren, and L. Svennerholm. 1977. Ultrastructural localization of cell membrane GM1 ganglioside by cholera toxin. *Proc. Natl. Acad. Sci. USA.* 74:141–145.

Hirai, M., R. Kawai-Hirai, T. Hirai, and T. Ueki. 1993.Structural change of jack bean urease induced by addition of surfactants studied with sychrotron-radiation small-angle x-ray scattering. *Eur. J. Biochem.* 215:55–61.

Hirai, M., T. Hirai, and T. Ueki. 1994. Growing process of scattering density fluctuation of a medium distance in hydrogel of poly(vinyl alcohol) under stretching. *Macromolecules* 27:1003–1006.

Hirai, M., R. Kawai-Hirai, T. Takizawa, S. Yabuki, T. Hirai, K. Kobayashi, Y. Amemiya, and M. Oya. 1995. Aerosol-OT reversed micellar formation at low water-surfactant ratio studied by synchrotron radiation small-angle x-ray scattering. *J. Phys. Chem.* 99:6652–6660.

Hirai, M., S. Yabuki, T. Takizawa, Y. Nakata, H. Mitomo, T. Hirai, S. Shimizu, K. Kobayashi, M. Furusaka, and K. Hayashi, 1995. Ganglioside structure in solution. *Physica B*, 213/214:748–750.

Israelachvili, J. N., D. J. Mitchell, and B. W. Ninham. 1976. Theory of self-assembly of hydrocarbon amphiphiles into micelles and bilayers. *J. Chem. Soc. Faraday Trans. II.* 72:1525–1568.

Kojima, H., H.-K. Yoshikawa, A. Katagiri, and Y. Tamai. 1988. Thermotropic behavior, and electronmicroscopic structures of mixtures of gangliosides and dipalmitoylphosphatidylcholine. *J. Biochem.* 103: 126–131.

Maggio, B., T. Ariga, J. M. Sturtevant, and R. K. Yu. 1985. Thermotropic behavior of glycosphingolipids in aqueous dispersions. *Biochemistry.* 24:1084–1092.

Maggio, B., T. Ariga, J. M. Sturtevant, and R. K. Yu. 1985. Thermotropic behavior of binary mixtures of dipalmitoylphosphatidylcholine, and glycosphingolipids in aqueous dispersions. *Biochim. Biophys. Acta.* 818: 1–12.

Marcus,D. M. 1984. A review of the immunogenic and immunomodulatory properties of glycosphingolipids. *Mol. Immunol.* 21:1083–1091.

Masserini, M., and E. Freire. 1986. Thermotropic characterization of phosphatidylcholine vesicles containing ganglioside G_{M1} with homogeneous ceramide chain length. *Biochemistry.* 25:1043–1049.

Masserini, M., P. Palestini, and E. Freire. 1989. Influence of glycolipid oligosaccharide and long-chain base composition on the thermotropic properties of dipalmitoylphosphatidylcholine large unilamellar vesicles containing gangliosides. *Biochemistry.* 28:5029–5034.

Makita, A., and N. Taniguchi. 1985. Glycosphingolipids. *In* Glycolipids. H. Wiegandt, editor. Elsevier, New York. 1–100.

Robert, E. H., and M. B. Robert. 1964. Studies on the ganglioside micelle. *Biochim. Biophys. Acta.* 84:435–440.

Sillerud, L. O., D. E. Schafer, R. K. Yu, and W. Konigsberg. 1979. Calorimetric properties of mixtures of ganglioside G_{M1} and dipalmitoylphosphatidylcholine. *J. Biol. Chem.* 254:10876–10880.

Spiegel, S., and P. H. Fishman. 1987. Gangliosides as bimodal regulators of cell growth. *Proc. Natl. Acad. Sci. USA.* 84:141–145.

Svennerholm, L., A. K. Asbury, R. A. Reisfeld, K. Sandhoff, K. Suzuki, G. Tettamanti, and G. Toffano, editors. 1994. Biological Function of Gangliosides. Elsevier, Amsterdam.

Ulrich-Bott, B., and H. Wiegandt. 1984. Micellar properties of glycosphingolipids in aqueous media. *J. Lipid Res.* 25:1233–1245.

Ueki, T., Y. Hiragi, M. Kataoka, Y. Inoko, Y. Amemiya, Y. Izumi, H. Tagawa, and Y. Muroga. 1985. Aggregation of bovine serum albumin upon cleavage of its disulfide bonds, studied by the time-resolved small-angle x-ray scattering technique. with synchrotron radiation. *Biophys. Chem.* 23:115–124.

Zamyatin, A. A. 1972. Protein volume in solution. *Prog. Biophys. Molec. Biol.* 24:107–123.